Phase–property study of semiconductor selenium

Part I *Single-phase system*

M. F. KOTKATA
Physics Department, Faculty of Science, Ain Shams University, Cairo, Egypt

For more than two decades, there has been a large demand to use amorphous selenium as a photoreceptor material in electrophotographic applications as well as in many other semiconductor devices. However, the published results characterizing a single-phase selenium always stimulate interest in the structural properties of such a lone-pair chalcogen material. This paper provides more pertinent information concerning the phase–property relation of a single-phase crystalline, amorphous, and liquid selenium.

1. Introduction

Among several photoreceptor materials such as ZnO, CdS, organic photoreceptors, amorphous silicon (a-Si) and amorphous selenium (a-Se), selenium is the most widely used for xerographic photoreceptors all over the world. An interesting switching phenomenon has also been observed in elemental selenium in the crystal, amorphous solid and amorphous liquid form. The high-pressure phase of a-Se has been found to be a superconductor. Because of these and other applications, selenium has become a material of considerable commercial importance, and there have been numerous efforts to elucidate its structural properties.

In contrast to elemental amorphous tetrahedral semiconductors (e.g. silicon and germanium), for which structural models are agreed upon, the elemental chalcogenide semiconductor selenium raises some difficulties, as can be judged from the lack of agreement among published results. For instance, reported resistivities of non-crystalline selenium range from 10^9–10^{17} Ω cm, i.e. a difference of eight orders of magnitude. A careful consideration of the effects of defects on the molecular structures responsible for the gap states in amorphous materials, elucidated the fact that strain-induced defects control the electronic properties of tathogens, while thermodynamic-induced defects control those of chalcogenides.

In fact, there has always been a great interest in studying the phase–property relations of materials. This report presents a better view of the interrelation between phase and property, taking into consideration previous results obtained from different measurements, as well as new experimental and theoretical field studies on crystalline, amorphous, and liquid selenium.

2. The nature of selenium

Selenium is a unique element which can be preserved in both the crystalline and glass phases at room temperature. These forms are differentiated by the range of order present; long-range order (LRO) in the crystals and short-range order (SRO) in the glasses. However, as the average coordination number, $\bar{Z}$, decreases ($\bar{Z} = 4$ for a-Si or a-GaAs, and $\bar{Z} = 2$ for a-Se) another possibility takes place; the range of the order can increase beyond that of second or third nearest neighbours. Thus, one might expect the existence of positional and compositional order in the 1–10 nm regime intermediate-range order (IRO). Indeed, there is evidence for such IRO in a-Se [1] and also in a-Si:F:H [2].

In the crystalline form, selenium is known to exist in three structural modifications [3–5]. The crystal structure of trigonal selenium (t-Se) consists of helical chains, Se_n, arranged parallel in a hexagonal array. The monoclinic (m-Se) and rhombohedral (r-Se) selenium are molecular crystals consisting of Se_8 and Se_6 ring molecules, respectively. A fourth allotrope, orthorhombic selenium (o-Se) has also been found [6], where the most realistic constituent is a chair-type Se_7 ring molecule [7, 8]. Both the chain and ring of t-Se and m-Se have the same first neighbouring distance, the same bond angle, and the same dihedral angle. They differ only in the manner in which the phase of the dihedral angle varies [9].

The electronic configuration of the selenium atom is $4s^2 4p^4$. Of the six available valence electrons, only two actually occupy covalent bonding states. The states of these two s-electrons are sufficiently low in energy that they do not participate in bonding; two p-electrons form covalent bonds, one to each neighbour on the chain, and the remaining two enter the non-bonding "lone-pair" (LP) state. The LP states are the highest filled states and form the valence band; while the empty p-antibonding states form the conduction band, Fig. 1 [10]. The exchanged repulsion between LP electrons on the adjacent selenium atoms, within the helical chain, constrains the magnitude of the dihedral angle (101°) near to 90° [11]. It is known that
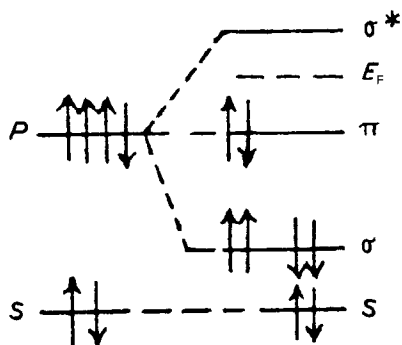
Figure 1 Bonding configuration of elemental selenium. The Fermi level, E_F, lies in the gap between the occupied $P\pi$ orbital and the unoccupied σ^* orbital.

there are covalent-like attractive bonds between chains arising from the overlap of an occupied LP(π) orbital on one selenium atom and the unoccupied p-like antibonding (σ^*) orbital on a neighbouring atom. Disorder in the chain arrangement reduces the $P\pi$-σ^* overlap and hence weakens the interchain bonds. In fact, the bonding character of a-Se is more anisotropic than that of t-Se [12, 13]. The weakening of interchain bonds leads to an appreciable degree of structural flexibility which may introduce various types of defect states. This means that a variety of intrinsic defects, with locally altered lattice structures, are easily produced by the injection of an electron or a hole and by a free terminal [14–16]. Electronic and lattice structures of terminal and internal defects in a Se chain are systematically studied [17, 18]. The fact that the uppermost filled band in a-Se, and other chalcogenide glasses, is not the bonding band as in a-Si (Fig. 2, [19]), but a band of states formed by LP electrons, is the major reason for the origin of the rather unusual defect chemistry in chalcogenide glasses, a negative correlation energy, self compensation, pinning of the Fermi level, and other defect-related phenomena that are almost absent in amorphous tetrahedral semiconductors [20, 21].

Neutron and X-ray diffraction measurements [22–24] indicate that the coordination of amorphous liquid selenium (l-Se) is nearly two and is weakly temperature dependent. As in a-Se, l-Se contains a mixture of ring and chain-like fragments [19].

Amorphous solid selenium can be easily prepared as a bulk glass (vitreous), by quenching it from the super-cooled melt where it usually exhibits a glass transition, or in the form of thin films, by depositing it from the vapour phase. The structure of the films is not different from that of bulk glass; it consists of the two molecular types: polymeric chains and monomeric rings. In the literature, several structural investigations on a-Se have been reported (cf. [1, 19, 25] and references therein); however, there have been difficulties in combining all features of the molecular morphology suggested by the various experiments into a single model. For instance, there is agreement that two neighbouring atoms at 0.232 nm and six second neighbours at about 0.369 nm exist; whereas beyond that there is little agreement on dihedral angles, bond angles, and particularly on the SRO in the form of

(a) Nearest neighbour distance
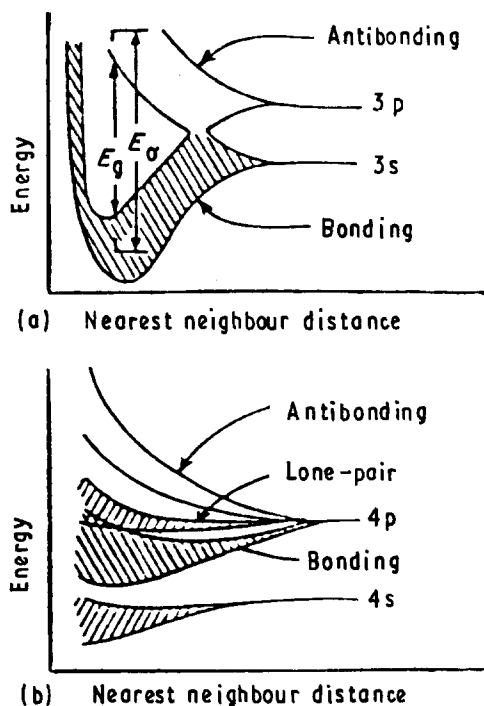
(b) Nearest neighbour distance

Figure 2 Sketch of energy bands against near-neighbour distance for (a) silicon as a tetrahedral semiconductor, and (b) selenium as an LP semiconductor.

rings or chains. Several researchers have attributed this lack of agreement, beyond the general difficulty of describing the atomic arrangement in the amorphous material, to the thermal history and specimen preparation condition [26]. A model is suggested for the distribution in the magnitude of the dihedral angle as a function of deposition conditions and annealing [27].

3. Sample preparation and experimental procedure

Spectroscopic elemental selenium, obtained from different manufacturers, all with purity 99.999% or better, was used for the preparation of the samples investigated.

Thin amorphous selenium films of different thicknesses lying in the range from 300–1000 nm were prepared by the thermal deposition technique under a pressure of 10^{-6} torr (1 torr = 133.322 Pa) on glass and/or quartz substrates using a coater unit (Edwards E306A). The measurements of transmittance, T, and the reflectance, R, were carried out at normal incidence and at room temperature, RT, in the spectrum range 400–2000 nm, using a spectrophotometer (Varian Cary 2390).

Amorphous bulk (glass) selenium samples were prepared by the melt-quenching technique. That is, 3–5 g selenium pellets were synthesized at a temperature T_s ($> T_m$), ranging from 250–1000 °C, for 2–3 h in Pyrex and/or quartz tubes sealed under vacuum (10^{-4}–10^{-6} torr) before subsequent quenching in iced water. The prepared selenium ingots were confirmed as non-crystalline using X-ray diffraction of a standard Philips diffractometer equipped with a fine focus CuK_α radiation source, and by differential thermal

analysis (Shimadzo DT-30) or differential scanning calorimetry (Mettler Thermosystem FP-84).

Crystalline selenium samples were prepared via two different thermal treatments: (i) selenium pellets encapsulated in Pyrex tubes at 10^{-4} torr were fused at 300 °C for 3 h and then left to cool in the oven at a rate of 0.8 °C min^{-1}, and (ii) the pelletes were also fused at 300 °C for 3 h and then rapidly transferred into a preheated oven adjusted to the required supercooling temperature, $T_{sc} = 80$–200 °C, for a period of 9 h (or 12 h) after which they were left to cool at a rate of 0.8 °C min^{-1}. The second method of preparation is expected to avoid formation of voids in the glass matrix which serve as heterogeneous nuclei when annealing starts from RT.

The details of the experimental arrangements and measuring techniques for structural and physical characterization of crystalline, amorphous solid (thin or bulk), and amorphous liquid selenium are those described in our previous publications for low softening, as well as highly resistive semiconductors [28–33]. Here, it is worth mentioning that the temperature range over which electrical measurements of a-Se can be made, is very limited by the high resistivity at low temperatures and the low glass transition temperature ($T_g < 50$ °C). The techniques considered include the hydrostatic density, Vicker's microhardness, differential thermal analysis (DTA) or differential scanning calorimetry (DSC), d.c. conduction, dielectric and optical measurements, photoconduction, and photothermal deflection spectroscopy (PDS).

4. Results and discussion

4.1. Density and microhardness

Fig. 3 shows the X-ray diffraction patterns of powdered samples for a melt-quenched (Fig. 3a) and well-crystallized (190 °C for 16 h, Fig. 3b) selenium. The former pattern shows no characteristic diffraction lines, revealing the absence of any regular crystalline structure. Instead, a fused hump characterizes the amorphous nature of the quenched phase. The latter reveals the Bragg angle dependence of diffraction line intensities of t-Se with the lattice parameters; $a = 0.43662$ nm and $c = 0.49536$ nm. The strongest line (100%) is (1 0 1) with interplanar spacing $d = 0.298$ nm. The Miller indices of the diffracting planes are given in this figure.

The values of the hydrostatic density of amorphous bulk (glassy) selenium (g-Se) and crystalline selenium (c-Se) are 4.28 and 4.75 g cm^{-3}, respectively. The deficit of density of the amorphous phase to that of the crystalline phase is mainly caused by an increase in the intrachain distances in the amorphous network.

The results of measuring the Vicker's microhardness (VH) of g-Se samples prepared by quenching from different temperature, T_s, are given in Fig. 4. The value of VH shows a decrease from 36 kg mm^{-2} to 28 kg mm^{-2} with increasing T_s from 250 °C to 1000 °C. The results [34, 35] obtained by studying the effect of T_s on both the degree of polymerization, P, gained from viscosity measurements, and the solubility, S, of g-Se in $C_2H_2I_2$ are also represented in Fig. 4. The decrease in the values of VH, P, and S with
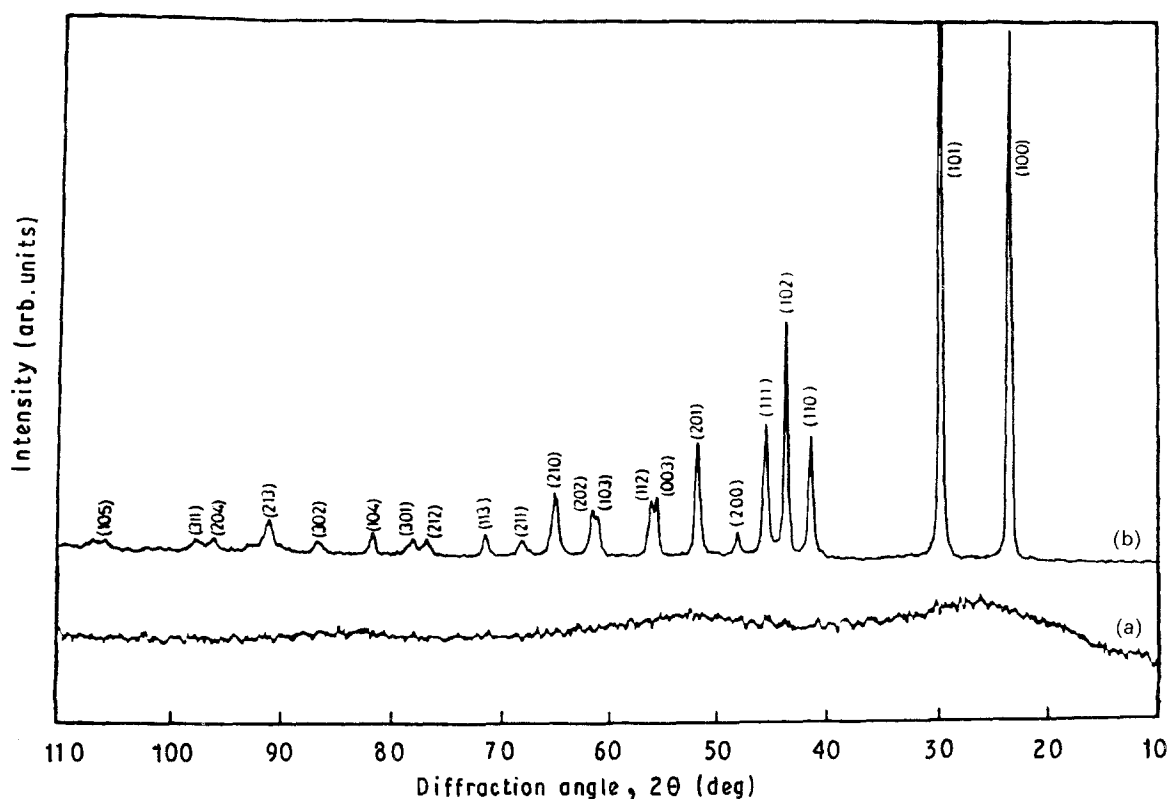

Figure 3 X-ray diffraction pattern of (a) iced-water quenched selenium, and (b) Bragg angle dependence of diffraction line intensities of a crystalline selenium sample.
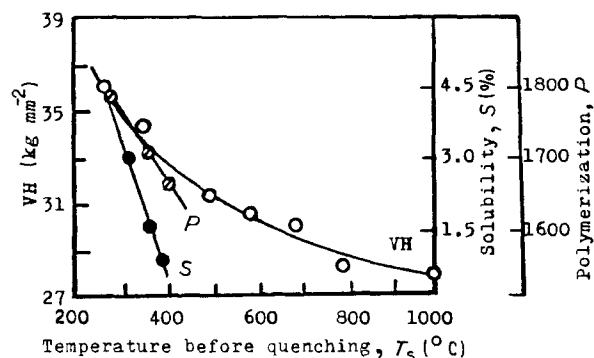
Figure 4 Dependence of room-temperature Vicker's microhardness of g-Se samples on the temperature before quenching, T_s. The dependence of the degree of polymerization, P, and the solubility, S, on T_s of g-Se are also represented (after [34, 35]).

increasing T_s argues a reduction in both the number of ring-shaped molecules and the average length of polymeric chains. The latter causes an increase in the number of chain ends, and hence the number of potential barriers in the frozen liquid. Accordingly, a definite molecular and electronic structure is expected for each T_s. On the other hand, the effect of gamma-radiation on the solubility of g-Se is reported [36].

4.2. Dielectric constant and d.c. conduction

A graphite measuring cell made of spectroscopically pure rods was designed for measuring the capacitance, C. The cell consists of two cylindrical graphite electrodes made coaxial at 1 mm spacing with the aid of a ceramic cover acting as a guard ring [31]. The measuring technique consists in determining, with the help of specially designed highly sensitive resonance circuit, the over-potential, Q, and the capacitance, C. The method depends on a comparison between the capacitance, C_o, of the cell empty, and the value, C, measured with the semiconducting material (selenium) inserted between its electrodes. The ratio C/C_o gives the relative dielectric constant, ε. The value of the capacitance was determined by using a Scherring bridge.

The dielectric measurements indicate that the value of the real part of the dielectric constant, ε_r, is 5.7 for g-Se and lies in the range 9.6–11 for c-Se depending on the crystallization condition [31]. The crystallization condition specifies the state corresponding to different grain sizes and define what is called the "degree of perfectness or crystallinity" (DPC) [30].

Measurements of the d.c. conductivity, σ, of selenium was done for samples either in the form of a wafer or enclosed under a vacuum of 10^{-4}–10^{-6} torr in a Pyrex tube provided with two tungsten electrodes near the base. The electrodes have a cross-sectional area of $\approx 0.1\ cm^2$ and separated by $\approx 0.1\ cm$. Also, glassy specimens with thickness between 0.2–1 mm were obtained from the quenched ingots by grinding and wet-polishing to optical quality for electrical measurements. Coaxial circular carbon-dag electrodes were applied to the sample faces to ensure good contacts. The area of each electrode was $\approx 1\ cm^2$ which nearly represents half of the sample area. In all geometrical cases, the conductivity was calculated

taking into consideration both the electrodes' separation and their cross-sectional area. A low stable voltage (< 5 V) was applied and a Keithley 616 digital electrometer was used for current measurements. The measurements were done under controlled equilibrium conditions, i.e. measurements were taken 30–45 min after the required temperature was attained.

Fig. 5 shows the temperature dependence of σ for the three single phases of selenium: glass (g-Se), crystal (c-Se), and liquid (l-Se). The figure shows the results for selenium samples prepared under different conditions, where the function $\sigma(T)$ was measured at temperatures below the glass transition value, $T_g \approx 48\ °C$, for the amorphous state to avoid any possible phase transformation, and at temperatures higher than the melting point, $T_m = 220\ °C$, for the liquid state. A plot of the function $\log \sigma = f(1/T)$ for each of the different single phases of selenium gave a straight line relationship reflecting the semiconducting behaviour of selenium and satisfying a thermally activated formula of Arrhenius type: $\sigma = \sigma_o \exp(-\Delta E/kT)$. As a function of the prepared condition of each selenium phase, Table I gives the characteristic electrical parameters, ΔE, the thermal activation energy of conduction, $\sigma(RT)$ the conductivity at $RT = 20\ °C$, and σ_o the pre-exponent factor (the intercept of the ordinate at $1/T = 0$).

As given in Table I, the value of $\sigma(RT)$ is very low [$\approx 10^{-14}\ (\Omega cm)^{-1}$] for samples g1-Se and g2-Se. This is almost the case for many other amorphous semiconductors with a wide band gap ($\geqslant 2$ eV). The corresponding values of ΔE (0.97–1.1 eV) are approximately equal to half the band gap of intrinsic a-Se [33, 37–40], indicating a pinning of the Fermi level near the mid-gap. A relatively high value of 8 $\times 10^{-9}\ (\Omega cm)^{-1}$ was, however, found for $\sigma(RT)$ of sample g3-Se. This can be attributed to the sensitivity of selenium to impurities, particularly oxygen, because such a relatively high value of $\sigma(RT)$ was recorded only for the glassy samples prepared under a vacuum of 10^{-4} torr. It was reported [41–43] that the incorporation of 50 p.p.m. O_2, added as SeO_2, to the melt increases $\sigma(RT)$ from 10^{-17} to $10^{-11}\ (\Omega cm)^{-1}$. A deoxygenating effect is observed with silicon and also with mercury, silver, bismuth and potassium. Mott and Davis [44] mentioned that the effects of these impurities on the resistivity are probably best attributed to structural modifications rather than to doping in the conventional sense.

A neutral dangling bond is a site at the end of the selenium chain at which one of the LP orbitals contains a single electron. It is now argued [16] that, if an electron is removed from one of the LP orbitals of a nearby atom in a neighbouring chain, the two singly occupied orbitals will form a bond; the two atoms will be attracted to each other and this second atom is now three-fold coordinated. The resulting defect, positively charged, was called by Street and Mott [14] a D^+ centre and by Kastner *et al.* [15] a C_3^+, denoting the three-fold coordination and the positive charge. If these defects exist in the glasses, or in the liquids from which they are quenched, there must be a correspond-
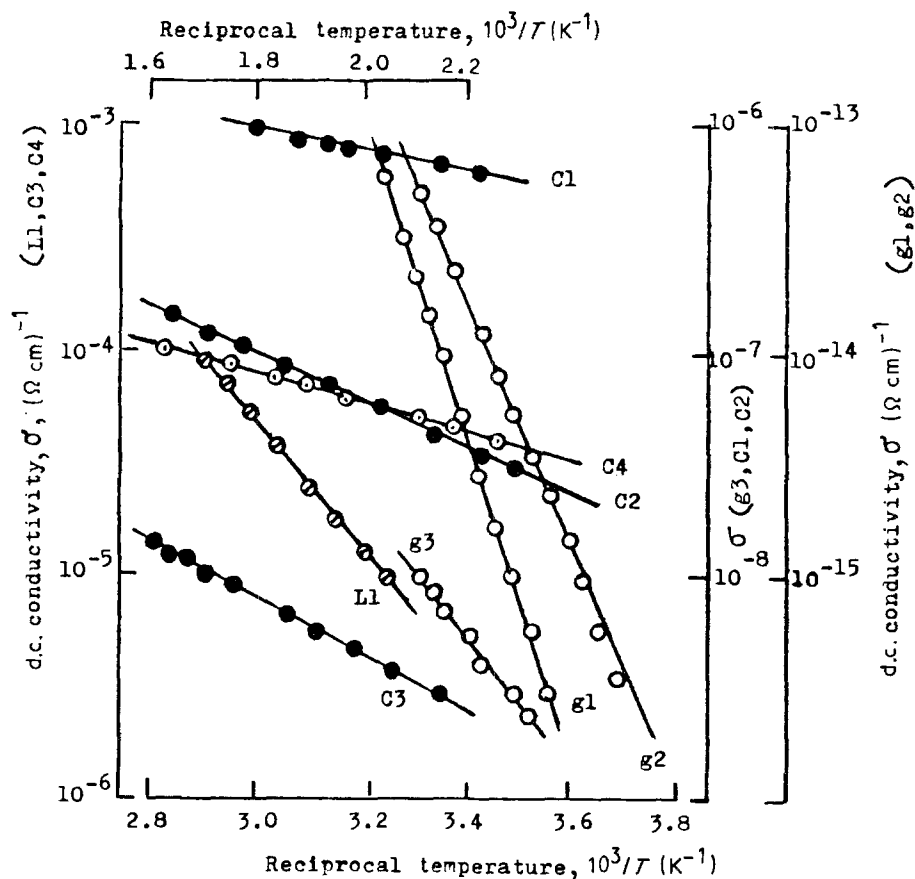
Figure 5 Temperature dependence of d.c. conductivity of different selenium samples in the three states: amorphous solid (glass, g-Se), amorphous liquid (l-Se), and crystalline (c-Se). 1-4, the different preparation conditions as given in Table I.

TABLE I Characteristic electrical parameters of single-phase selenium samples as a function of preparation conditions

Phase	Symbol	Preparation conditions	$-\operatorname{Log}\sigma(\mathrm{RT})^*$	$\operatorname{Log}\sigma_o{}^*$	ΔE (eV)
Glass	g1-Se	Product 1, 350 °C for 3 h (10^{-6} torr, quartz tube), iced-water quenching	13.9	5.6	1.10
	g2-Se	Product 2, 350 °C for 3 h (10^{-6} torr, quartz tube), iced-water quenching	14.6	3.3	0.97
	g3-Se	Product 1, 350 °C for 3 h (10^{-4} torr, Pyrex tube), iced-water quenching	8.1	2.0	0.58
Liquid	l1-Se	Product 1 (10^{-4} torr, Pyrex tube)	–	– 0.05	0.55
Crystal	c1-Se	Gradually cooled from 300 °C to RT with a rate of 0.8 °C min^{-1}	6.1	– 4.4	0.10
	c2-Se	Transferred from 300 °C to T_{sc} = 100 °C and held for 9 h before cooling to RT at a rate of 0.8 °C min^{-1}	7.4	– 1.6	0.33
	c3-Se	As above, but at T_{sc} = 125 °C	5.5	– 0.5	0.29
	c4-Se	As above, but at T_{sc} = 170 °C	4.3	– 1.3	0.17
	t-Se	Single crystal [after 50]	4-5	–	0.15 eV/molecule

* σ is measured in $(\Omega\ \mathrm{cm})^{-1}$

ing negative centre; the electron must go somewhere. The obvious place for it is another, perhaps distant, dangling bond, producing the C_1^- (or D^-) centre, Fig. 6 [45]. If these centres are to exist in preference to the neutral dangling bonds, the reaction

$$2C_1^0 \rightarrow C_3^+ + C_1^- \qquad (1)$$
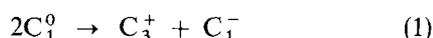
must be exothermic. This is sometimes described as a result of a "negative Hubbard U", the repulsion $\langle e^2/kr_{12}\rangle$ between the two electrons in the dangling bond being more than compensated by the energy gained as the material contracts locally to form three-fold co-ordinated selenium [16]. Kastner *et al.* [15]

argued that this must be so, because each broken bond (C_1^-) is always associated with an extra bond formed at C_3^+. The bond energy is high, and structures with uncompensated broken bonds will be avoided. However, the conjugate pair of charged states (C_1^- and C_3^+) can be created by a bond switch from an interchain to an intrachain position.

The sensitivity of selenium was also examined by infrared spectroscopy [41] where the addition of 500 p.p.m. O_2 caused the appearance of new absorption bands in the spectrum of pure deoxygenated a-Se and related to SeO_2 bonds. It was suggested that oxygen bonds to the D^- centres and not to the D^+
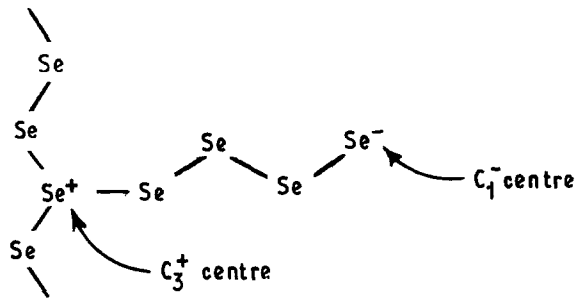
Figure 6 Valence alternation pairs (VAPs) of a-Se (after [45]).

which are already strongly bonded to another selenium [45]. These authors argued also that the increase in $\sigma(RT)$ is caused by a decrease in ΔE and even without an associated reduction in the optical gap. In the studied case, the increase in $\sigma(RT)$ from 1.4×10^{-14} $(\Omega\,cm)^{-1}$ to 8×10^{-9} $(\Omega\,cm)^{-1}$ is accompanied by a decrease in ΔE from 1.1 eV to 0.58 eV. Thus, it seems that oxygen impurity acts by shifting the Fermi level due to changing the equilibration of structural defects as a result of the neutral electrical condition.

It seems also that the presence of oxygen influences the value of σ_o as it drops from 4×10^5 $(\Omega\,cm)^{-1}$ for g1-Se to 10^2 $(\Omega\,cm)^{-1}$ for g3-Se. Assuming that oxygen leads to a decrease in σ_o by a factor of $\exp(-\gamma/k)$, where k is the Boltzmann constant, γ would give a value of 3.14×10^{-4} $eV\,K^{-1}$. Here, oxygen acts as a dopant because similar phenomena have been detected by the addition of phosphorus and tellurium to a-Si:H [46] and a-GaAs:H [47], respectively.

On the other hand, the effect of oxygen on electrophotographic properties of selenium has been systematically investigated by Onozuka and Oda [48], and they found that the increase in oxygen decreases the residual potential in the positive charge mode and increases it in the negative charge mode. These authors explained their experimental results by the modified structural defect model in a-Se [14, 15], i.e. by the relative concentration of C_1^- to C_3^+. The increase in oxygen concentration increases C_3^+ and decreases C_1^- when its content exceeds a threshold value. That is, oxygen atoms change the concentration of native charged defects indirectly and they themselves act as shallow hole traps when they are bonded to native selenium defects.

Measurements of $\sigma = f(T)$ for selenium in its liquid phase indicated a value of $\Delta E = 0.55$ eV in the temperature range 230–370 °C. Previous work on l-Se gave values of 0.25–0.57 eV below 500 °C [49]. It seems that the defect conduction prevails below 500 °C. The value of the measured ΔE depends on the type and density of these defects.

Measurements of the photoconductivity and photo-e.m.f. of l-Se indicate the presence of discrete states in the band gap [51]. Electron spin resonance (ESR) and magnetic susceptibility experiments [52, 53] indicated, respectively, an activation energy of 0.63 and 0.87 eV for the defect centres. The presence of such centres is probably responsible for the conduction mechanism in l-Se. It can be concluded that there is a definite molecular structure for each temperature of l-Se and

this structure is preserved when the melt is rapidly cooled [54, 55]. The length of the chains decreases exponentially with increasing temperature [34, 38, 53]. This causes an exponential increase in the number of chain ends and hence the number of potential barriers. It is therefore possible to prepare samples of a-Se having certain predicted properties by controlling the temperature of the melt.

Crystallization of a-Se can occur from the supercooled liquid state in the midrange of temperature between the glass transition temperature $T_g \approx 48$ °C [56] and the melting temperature of t-Se, $T_m = 221.2$ °C [57]. This melt crystallization involves initial crystallization of the macromolecules Se_n through chain folding [58]. This is followed by ring opening and crystallization during polymerization of the remaining Se_8 [59, 60].

Upon crystallization, the value of $\sigma(RT)$ increases and lies in the range 2×10^{-8}–3.8×10^{-5} $(\Omega\,cm)^{-1}$ depending on the considered scheme of crystallization, Table I. Other researchers [61] published a value of 1.5×10^{-5} $(\Omega\,cm)^{-1}$ for c-Se prepared by the transfer from the melt to an oven preheated at $T_{sc} = 125$ °C.

The scattering of $\sigma(RT)$ values from one crystallized sample to another, depending on the scheme of thermal preparation, is evidently due to their degree of perfectness of crystallinity (DPC). The dependence of the latter on T_{sc} has been studied by X-ray diffraction [30]. The results indicated that the supercooling of l-Se at $T_{sc} = 190$ °C for 16 h, led to an X-ray diffraction pattern of lines having maximum intensities and sharpness. The height of the peaks of this pattern was therefore taken as a reference to calculate the DPC of other selenium samples crystallized at lower or higher values of T_{sc}. Here, it is worth mentioning that the introduction of the idea of the DPC means that polycrystalline selenium cannot be considered as a mixture of crystalline and amorphous phases, but it is essentially a crystalline material of various grain sizes. Every grain, of course, has several unit cells; if the grain contains at most one unit cell, the amorphous structure of selenium is reached.

Considering the above fact that the crystallized material is essentially a crystalline material of various grain sizes, Fig. 7 shows the effect of supercooling temperature, T_{sc}, on the structural environment of selenium crystallized for 9 h. The T_{sc} dependence of DPC for the two planes (1 0 1) and (2 0 1) of supercooled l-Se samples annealed for 9 h is shown in Fig. 7c. The value of DPC increases from 25%–30% to 97% as T_{sc} rises from 100 °C to 190 °C. A similar behaviour has been detected for the grain size, V, which increases markedly with increasing T_{sc} up to 190 °C, Fig. 7a. It is worth noting that 9 h annealing at $T_{sc} = 80$ °C was not sufficient to modify greatly the SRO of the supercooled l-Se, where X-ray diffraction indicated that the resulting material has a microcrystalline structure with IRO, with a linear dimension of the crystallites of < 10 nm. Annealing for larger periods improves the grain sizes of the crystallites. The increase in $\sigma(RT)$ with T_{sc} (Fig. 7d) matches the increase in the crystallite size well (Fig. 8) as the latter minimizes the dielectric path for charge carriers be-
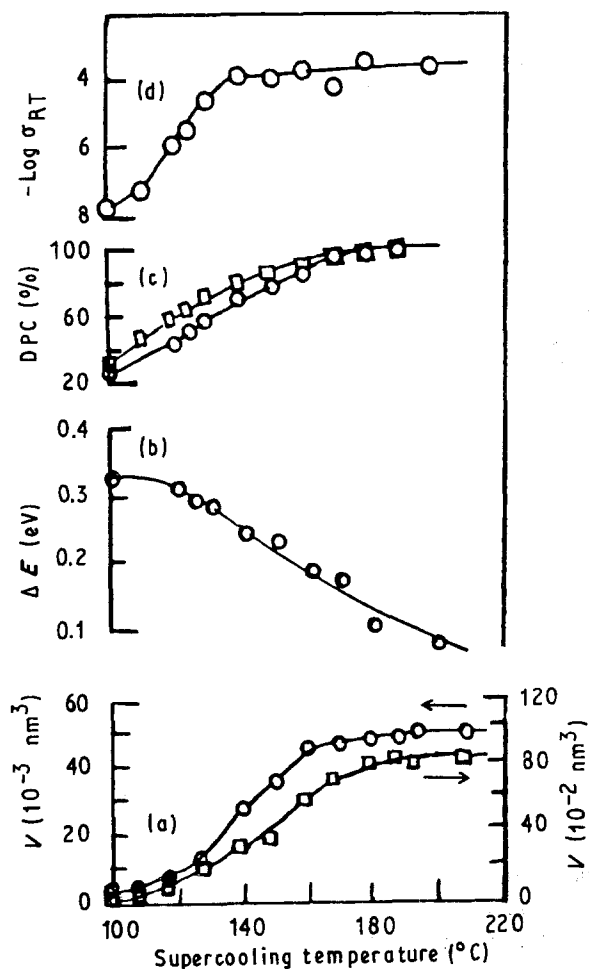
4852

Figure 7 The supercooling-temperature (T_{sc}) dependence of (a) the grain size, (b) activation energy, (c) DPC, and (d) $\log \sigma(RT)$ of supercooled l-Se samples annealed for 9 h before cooling at a rate of $0.8\,°C\,min^{-1}$. (O) plane (1 0 1), (□) plane (2 0 1).

As mentioned above, selenium crystallizes from the amorphous phase by chain folding, so that the poly-crystalline selenium is likely to have lamellar regions within the crystallites. Thickening between these lamellae can occur at higher temperatures [60] which would be expected to increase the perfectness of the crystallite, i.e. increasing the DPC, lowering the activation energy by increasing the ease of mobility of the charge carriers. In other words, the transition of the current carriers from one grain to another represents an energy barrier for the current carriers, assuming that the conductivity process takes place mainly at the surface of the grains. This means that this barrier decreases as the volume of the grain increases, leading to a decrease in ΔE. Fig. 9 shows the dependence of ΔE on grain radius, r, for the two planes (1 0 1) and (2 0 1) of c-Se prepared by annealing supercooled l-Se samples for 9 and 12 h. The value of ΔE increases almost linearly with decreasing radius, r, of the single grain (crystallite). Moreover, the rate of this decrease is independent on the length of anneal, 9 or 12 h, but it changes from plane (1 0 1) to plane (2 0 1).

However, the increase in conductivity is, in principle, due to the increase in diffusional length, L, density of charge carriers, and/or mobility. The conductivity increases about four orders of magnitude in the region of the grain volume from about 3.5×10^3 nm^3 to 35.6 $\times 10^3$ nm^3 with respect to the plane (1 0 1) for the c-Se samples annealed for 9 h. This corresponds to an increase in mobility by about two orders of magnitude and in diffusional length by about twice. Here, the value of L is considered to be half of the circumference of the grain [30]. Between 35.6×10^3 and 50 $\times 10^3$ nm^3, the effect of mobility is reversed. At a grain volume of 35.6×10^3 nm^3 and more, the diffusional length and the mobility reach their limiting contributions in such a manner that the increase in grain size ceases to affect the conductivity. The latter is almost constant in the temperature range of T_{sc} = 140–200°C, $\sigma(RT) \approx 1.3 \times 10^{-4}$ $(\Omega\,cm)^{-1}$, Fig. 8.

tween electrodes. Increasing the grain size leads to a reduction in the number of grains per unit volume and, consequently, the number of potential barriers across the charge carriers path. This explains the observed decrease in ΔE with increasing T_{sc}, Fig. 7b.
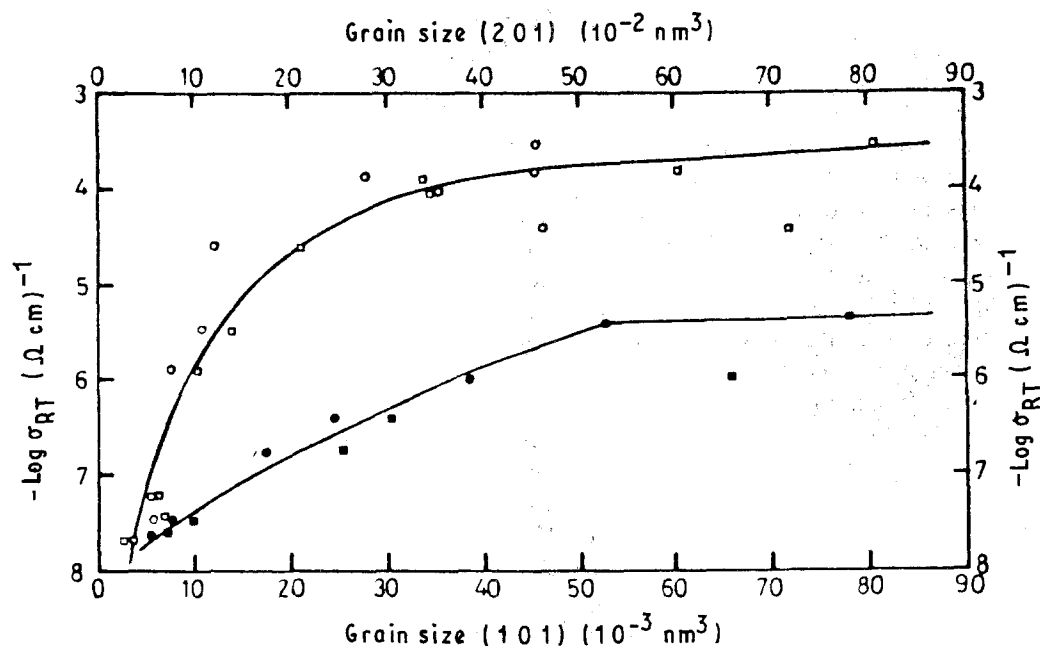

Figure 8 The grain size dependence of $\sigma(RT)$ of c-Se. (●, O) plane (1 0 1), (■, □) plane (2 0 1); (O, □) 9 h, (●, ■) 12 h anneal at T_{sc}.
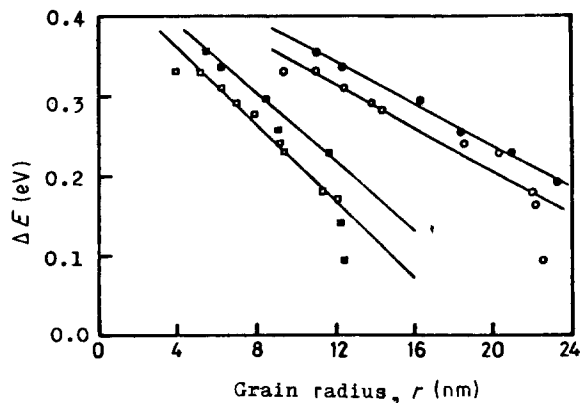
Figure 9 The dependence of the activation energy, ΔE, on the grain radius, r, of c-Se. ($\bullet$, $\bigcirc$) plane (1 0 1), ($\blacksquare$, $\square$) plane (2 0 1); ($\bigcirc$, $\square$) 9 h, ($\bullet$, $\blacksquare$) 12 h anneal at T_{sc}.

Accordingly, the process of increasing the grain size affects the electrical transport by the resultant of two factors: the decrease in the total area available per unit volume (i.e. the increase of the DPC), and the increase of the diffusional length (free path) with the consequent changes of the mobility of charge carriers. The latter depends on the holding condition of supercooling (temperature and time) and on the nature of the scattering mechanism in the polycrystalline matrix of selenium.

On the other hand, one of the primary differences between the $\sigma(T)$ behaviour of poly-crystalline and single-crystalline selenium is the hysteresis observed in the temperature dependence of σ between the heating and cooling curves of the same cycle. In general, conductivity measured on heating is lower than that measured on cooling. Such hysteresis effects have been shown to be a result of changing the mobility of the charge carriers and is related to structural changes in the solid [60]. These authors have mentioned that the activation energy for mobility of c-Se is almost equal to the total activation energy for conduction.

4.3. Photoconduction

For photoelectrical measurements, samples in co-planar configuration were used. 0.1 μm thick gold electrodes were evaporated on to the surface of the samples and the gap was about 300 μm wide. A xenon lamp (150 W) with interference filters was used as illumination source for the photoresponse experiments. The applied electrical field was in the range 10^3-10^4 V cm^{-1}. The photoresponse curves were normalized to a constant number of 10^{13} cm^{-2} s^{-1} incident photons. Prior to the experiments, the dark current versus applied voltage curves for each sample were plotted to ensure ohmic behaviour. In addition to the standard lock-in technique, a digital storage oscilloscope was used in steady state and transient photo-current measurements [62]. The recorded data were considered when the photocurrent, I_{ph}, reached its equilibrium value. Fig. 10 shows the temperature dependence of the photoconductivity, σ_{ph}, for a g1-Se sample. Such a function exhibits a maximum at a certain temperature ($T_{max} \approx 18\,°C$). This T_{max} marks a
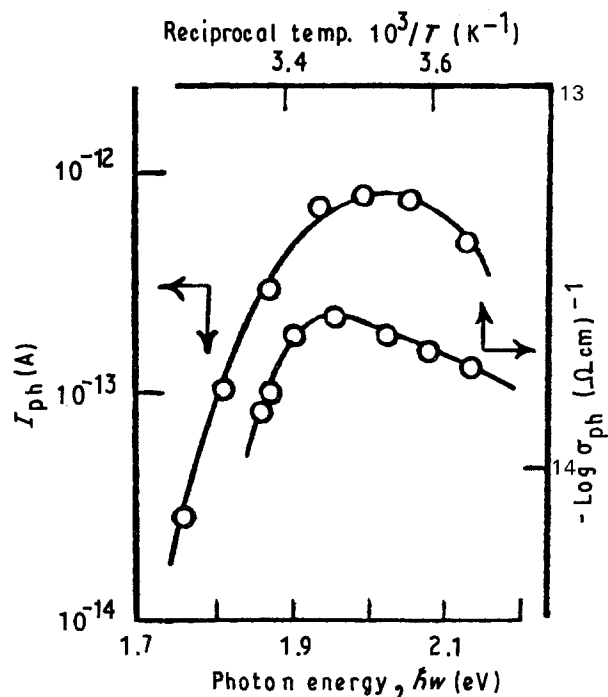

Figure 10 (a) The photon energy dependence of photocurrent, I_{ph}, and (b) the temperature dependence of photoconductivity, σ_{ph}, of g1-Se sample.

transition between two recombination regimes over which the I_{ph} depends exponentially on $1/T$(K) [44]. Here, it is worth noting that the nearly temperature-independent regime, commonly observed in chalcogenide glasses [63], is not reached because of the limitation for lower current measurements in the low temperature range.

The respective calculated values for the activation energies, ΔE, are 0.93 and 0.15 eV above and below T_{max}. The second value is close to the drift mobility activation energy of a-Se [64]. The first value corresponds to the high-temperature regime in which the photocurrent is less than the dark current and is proportional to the light intensity and thus to G (the number of carrier pairs generated per unit time per unit volume) [44]. The rate of recombination is then determined by the dark concentration of carriers. In the second regime, where the photocurrent is greater than the dark current, recombination is between electrons and holes, both of which are generated by illumination. In this regime, I_{ph} is proportional to $G^{1/2}$; although it was reported [65] that in chalcogenide glasses at low intensities, I_{ph} is proportional to G.

However, assuming on both sides of T_{max}, that the photocurrent is carried in the extended states, the change in ΔE values would reflect the variation in trapping and recombination kinetics determined by the density and nature of gap states.

The spectral response of I_{ph} is also shown on Fig. 10. The I_{ph} has a maximum value at a photon energy corresponding to the onset of the interband electronic transition and falls at both lower and higher energies. This has also been observed for many other bulk quenched materials [66, 67]. The decrease in I_{ph} at energies higher than E_g (i.e. > 2 eV, see next section) indicates that surface recombinations differ

from those in the bulk material. It seems that the exposure to oxygen damages the molecular structure of a layer of few micrometres at the surface of the bulk samples.

4.4. Optical properties and PDS

The spectral distribution curves (transmittance, T, and reflectance, R) have been recorded at normal incidence and at RT in the spectrum range 400–2000 nm for a-Se films 320–520 nm thick. The films were prepared by vacuum deposition on to glass and/or quartz substrates under a pressure of 10^{-5} torr [33]. Fig. 11 shows the photon energy, hw, dependence of both the imaginary part of the complex dielectric constant, ε_2, and the absorption coefficient, α, for 450 nm a-Se film. It is seen that the absence of LRO in the amorphous network spreads out the fine structure of the ε_2 spectrum: the maximum appearing at 2.2 eV in the ε_2 spectrum of c-Se [68] is spread out from the amorphous spectrum, and instead there is a broad structure. A shift of the absorption edge to higher energies is also detected, Fig. 11a. Fig. 11b indicates that the absorption edge is rather flat and decays approximately exponentially with energy.

Above the exponential absorption edge, the form of the absorption coefficient in a-Se obeys the relation

$$\alpha hw \approx \varepsilon_2 (hw)^2 \propto (hw - E_g) \qquad (2)$$

In this respect, a good straight line is obtained on a plot of $\varepsilon_2(hw)^2$ against hw in Fig. 12, and an optical gap E_g of magnitude 2 eV is obtained by extrapolation. In contrast to amorphous tetrahedral semiconductors, for which the relation $\alpha hw = f(hw - E_g)^2$ is linear [47, 69], a-Se does not exhibit a fairly linear

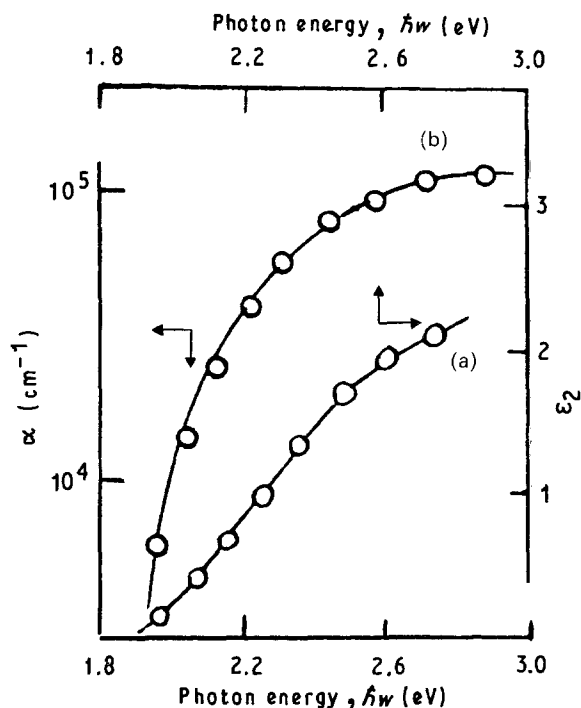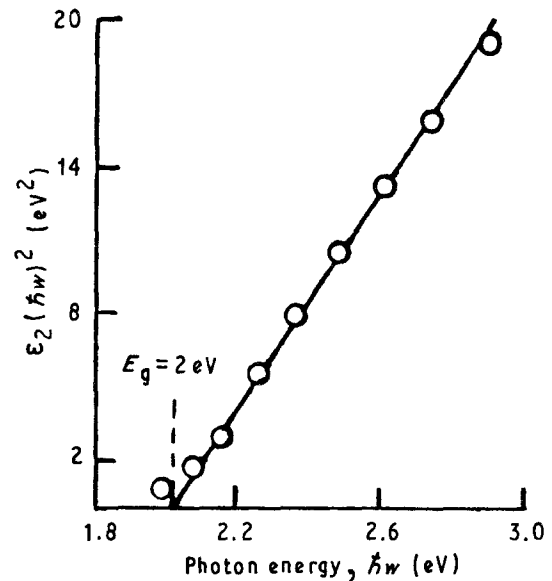*Figure 12* The photon energy dependence of $\varepsilon_2(hw)^2$ for a-Se film (450 nm).

relationship over all the energy range considered. This is believed to arise from a sharp increase in the density of states at the band edge [37], a possibility suggested by the one-dimensional nature of the chain-like structure of selenium [44]. The value of E_g (2 eV) calculated from Fig. 12 agrees with those published elsewhere; 1.97–2.08 eV [37, 38, 70]. Here, it is worth mentioning that changing the preparation conditions modifies E_g.

To detect the very weak optical absorption levels in a-Se, the spectral distribution of the sub-gap states has been determined by photothermal deflection spectroscopy (PDS). The basis of this technique was given by Amer and Jackson [71]. Fig. 13 shows the spectral distribution curves as recorded by both PDS and transmission for a-Se film (966 nm thick). These data were taken at RT for films prepared by thermal deposition under a pressure of 10^{-6} torr. The absorption edge spectra of the figure indicates a large density of states in the pseudo-gap. The value of the slope of the Urbach edge is overestimated because there is probably a continuation of the defect absorption in this spectral range.

The values of the characteristic parameters obtained from the analysis of the distribution curves of Fig. 13 are: 2.53 for n (the refractive index of the film at $\lambda = 2000$ nm), 2.03 eV for E_g (the optical gap at $\alpha = 10^4$ cm^{-1}), and 102 meV for E_o (the energy of Urbach edge, determined from the slope of $\log \alpha$ against hw (eV) in the exponential part of the edge). Details of the measuring arrangement and data evaluation are given by Theye *et al.* [72].

5. Conclusion

A systematic investigation for the phase–property relations of the elemental chalcogen semiconductor selenium reveals some interesting points.

1. The decrease in the values of Vicker's microhardness (VH), together with both polymerization, P, and solubility, S, with increasing temperature of synthesis, T_s, argues a reduction in both the number of

Figure 11 The photon energy dependence of (a) the imaginary part of the dielectric constant, ε_2, and (b) the absorption coefficient, α, for a-Se film (450 nm).
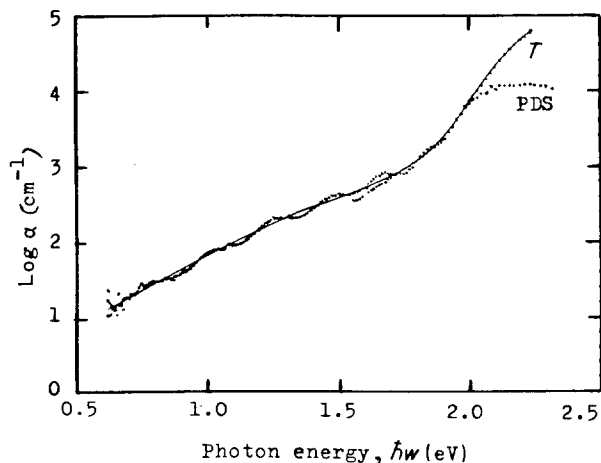
Figure 13 Typical photothermal deflection spectroscopy (PDS) and transmission, T, distribution curves of a-Se film (966 nm).

ring-shaped molecules and the average length of polymeric chains.

2. Reducing the pressure inside the ampoules to 10^{-6} torr, during the synthesis, renders non-crystalline selenium to its intrinsic state of conduction. Oxygen coming from ampoules sealed under higher pressure (10^{-4} torr) dramatically affects the resistivity, activation energy, and pre-exponential factor. The thermal history and the temperature before quenching were also detected to influence the structure resulting in a lack of agreement between results published by several researchers.

3. The electrical conductivity of l-Se suggests defect conduction below 500 °C as estimated from the measured value of the activation energy.

4. The value of $\sigma(RT)$ of c-Se samples (prepared at different supercooling temperatures, T_{sc}) reflects the dependence of the degree of perfectness of crystallinity (DPC) on T_{sc}. Rising T_{sc} increases the crystallite size and thereby reduces the high resistive amorphous path between electrodes. It leads also to a reduction in the number of grains per unit volume and, consequently, in the number of potential barriers across the conduction path. A simple model is presented in the text for interpreting the results which correlates the structural environment with the electrical transport properties.

5. The photoconductivity measurements reveal two temperature-dependent regimes with two different activation energies, 0.93 and 0.15 eV, below and above a critical temperature (18 °C). The value of the photoconductivity gap is found to be 2 eV.

6. A combination of photothermal deflection spectroscopy (PDS) and transmission measurements indicates a large density of states in the pseudo-gap due to the observed shoulder at low energies. Also, there is probably a continuation of the defect absorption in this spectral range. The characteristic energy values of the optical gap, E_g, and the Urbach edge, E_o, are evaluated to be 2.03 eV and 102 meV, respectively. The former matches well the value of the photoconductivity gap, 2 eV.

References

1. T. TAKAHASHI, K. OHNO and Y. HARADA, *Phys. Rev.* **B21** (1980) 3399.
2. R. TSU, M. IZU, S. R. OVSHINSKY and F. H. POLLAK, *J. de Phys.* **42** (1981) C4-269.
3. A. F. WELLS, "Structural Inorganic Chemistry", 4th Edn (Clarendon Press, Oxford, 1975) p. 572.
4. Y. MIYAMOTO, *Jpn J. Appl. Phys.* **19** (1980) 1813.
5. T. TAKAHASHI, K. MURANO, K. NAGATA and Y. MIYAMOTO, *Phys. Rev.* **B28** (1983) 4893.
6. K. NAGATA, H. TASHIRO and Y. MIYAMOTO, *Jpn J. Appl. Phys.* **20** (1981) 2265.
7. K. NAGATA and Y. MIYAMOTO, *Jpn Appl. Phys.* **23** (1984) 704.
8. T. TAKAHASHI, S. YAGA, T. SAGAWA, K. NAGATA and Y. MIYAMOTO, *J. Phys. Soc. Jpn* **54** (1985) 1018.
9. J. ROBERTSON, *Phil. Mag.* **34** (1976) 13.
10. *Idem., Adv. Phys.* **32** (1983) 461.
11. Y. KATYAMA, M. YAO, Y. AJIRO, M. INUI and H. ENDO, *J. Phys. Soc. Jpn* **58** (1989) 1811.
12. C. S. KIM and P. BOOLCHAND, *Phys. Rev.* **B19** (1979) 3187.
13. G. LUCOVSKY and C. K. WONG, *Phil. Mag.* **B52** (1985) 331.
14. R. A. STREET and N. F. MOTT, *Phys. Rev. Lett.* **35** (1975) 1293.
15. M. KASTNER, D. ADLER and H. FRIZSCHE, *ibid.* **37** (1976) 1504.
16. N. F. MOTT, "Conduction in Non-Crystalline Materials" (Clarendon Press, Oxford, 1987).
17. A. IKAWA and H. FUKUTOME, *J. Phys. Soc. Jpn* **58** (1989) 4517.
18. *Idem., ibid.* **59** (1990) 1002.
19. H. FRITZSCHE, in "Physical Properties of Amorphous Materials", edited by D. Adler, B. B. Schwartz and M. C. Steele (Plenum Press, London, 1985) p. 313.
20. R. STEUDEL, *J. Non-Cryst. Solids* **83** (1986) 63.
21. S. O. KASAP, B. POLISCHUK and V. AIYAH, *J. Appl. Phys.* **67** (1990) 1918.
22. J. MOSCINSKI, A. RENNINGER and B. L. AVERBACH, *Phys. Lett.* **A42** (1973) 453.
23. M. MISAWA and K. SUZUKI, *Trans. Jpn Inst. Metals* **18** (1977) 427.
24. R. BELLISENT and G. TOURNAND, *J. Non-Cryst. Solids* **35** (1980) 1277.
25. B. W. CORB, W. D. WEI and B. L. AVERBACH, *ibid.* **53** (1982) 29.
26. S. O. KASAP and C. J. JUHASZ, *Photogr. Sci. Engng* **26** (1982) 239.
27. P. J. CARROLL and J. S. LANNIN, *Solid State Commun.* **40** (1981) 81.
28. M. F. KOTKATA, M. H. EL-FOULY, A. Z. EL-BEHAY and L. A. EL-WAHAB, *Mater. Sci. Engng* **60** (1983) 163.
29. M. F. KOTKATA and M. K. EL-MOUSLY, *Acta Phys. Hung.* **54** (1983) 303.
30. M. F. KOTKATA and M. H. ALY, *Ind. J. Tech.* **22** (1984) 170.
31. M. F. KOTKATA, H. A. KHALEK, W. M. ATIA, T. PORJESZ and M. EL-SAMAHY, *J. Mater. Sci.* **20** (1985) 2973.
32. M. F. KOTKATA and K. M. KANDIL, *Mater. Sci. Engng* **95** (1987) 287.
33. M. F. KOTKATA and F. A. EL-WAHAB, *J. Mater. Sci.* **25** (1990) 2379.
34. A. EISENBERG and A. V. TOBOLSKY, *J. Polym. Sci.* **46** (1960) 19.

35. G. LUCOVSKY, in "The Physics of Selenium and Tellurium", edited by E. Gerlach and P. Grosse (Springer-Verlag, New York, 1979) p. 179.

36. I. A. DOMORYAD, M. G. SPIRINA and N. I. TIMO-CHINA, *J. Non-Cryst. Solids* **90** (1987) 525.

37. E. A. DAVIS, *ibid.* **4** (1970) 107.

38. J. P. AUDIERE, C. H. MAZIERES and J. C. CARBALIES, *ibid.* **27** (1978) 411.

39. S. CHAUDHURI, S. K. BISWAS, A. CHOUDHURY and K. GOSWAMI, *ibid.* **46** (1981) 171.

40. S. K. AL-ANI and C. A. HOGARTH, *ibid.* **69** (1984) 167.

41. W. C. LACOURSE, V. A. TWADDELL and J. D. MACK-ENZIE, *ibid.* **3** (1970) 234.

42. V. A. TWADDELL, W. C. LACOURSE and J. D. MACK-ENZIE, *ibid.* **8–10** (1972) 831.

43. O. ODA, A. ONOZUKI and I. TSUBOYA, *ibid.* **83** (1986) 49.

44. N. F. MOTT and E. A. DAVIS, "Electronic Processes in Non-Crystalline Materials", 2nd Edn (Clarendon Press, Oxford, 1979).

45. D. ADLER, in "Physical Properties of Amorphous Materials", edited by D. Adler, B. B. Schwartz and M. C. Steele (Plenum Press, London, 1985) p. 5.

46. D. A. ANDERSON and W. PAUL, *Phil. Mag.* **B45** (1982) 1.

47. K. SEDEEK and H. CARCHANO, *J. Appl. Phys.*, to be published.

48. A. ONOZUKA and O. ODA, *J. Non-Cryst. Solids* **116** (1990) 219.

49. H. GOBRECH, F. MAHALJURI and D. GAWLIK, *J. Phys. C* **4** (1971) 2247.

50. J. STUKE, in "Selenium", edited by R. A. Zingaro and W. C. Cooper (Van Nostrand, New York, 1974) p. 174.

51. A. A. AIVAZOV and B. G. BUDAGYAN, *Sov. Phys. Semicond.* **18** (1984) 1186.

52. D. C. KONINGSBERGER, J. H. VONWOLPUT and P. C. RIETER, *Chem. Phys. Lett.* **8** (1971) 145.

53. C. H. MASSEN, A. G. WEJTS and J. A. POULIS, *Trans. Farad. Soc.* **60** (1964) 317.

54. A. I. POPOV, *J. Phys. C* **9** (1976) L675.

55. M. F. KOTKATA, *J. Mater. Sci.* **26** (1991) 4869.

56. *Idem., ibid.*, **27** (1992) 4858.

57. H. C. SHU, U. GAUR and B. WUNDERLICH, *J. Polym. Sci. Polym. Phys. Ed.* **18** (1980) 449.

58. R. G. CRYSTAL, *J. Polym. Sci.* **8** (1970) 2153.

59. M. C. COUGHLIN and B. WUNDERLICH, *J. Polym. Sci. Polym. Phys. Ed.* **11** (1973) 1735.

60. K. E. MURPHY, B. B. WUNDERLICH and B. WUNDER-LICH, *J. Phys. Chem.* **86** (1982) 2827.

61. C. H. CHAMPNESS and R. H. HOFFMAN, *J. Non-Cryst. Solids* **4** (1970) 138.

62. M. F. KOTKATA, M. FÜSTOSS-WEGNER, L. TOTH, G. ZENTAI and S. A. NOUH, to be published.

63. J. G. SIMMONS and G. W. TAYLOR, *J. Phys. C* **7** (1974) 3051.

64. J. M. MARSHALL and A. E. OWEN, *Phil. Mag.* **31** (1975) 1341.

65. T. C. ARNOLDUSSEN, C. A. MENEZES, Y. NAKAGAWA and R. H. BUBE, *Phys. Rev.* **B9** (1974) 3377.

66. B. T. KOLOMITES and V. M. LYUBIN, *Phys. Status Solidi* **A17** (1973) 11.

67. E. A. FAGEN and H. FRITZCH, *J. Non-Cryst. Solids* **2** (1970) 180.

68. J. STUKE, *ibid.* **4** (1970) 1.

69. L. CHAHED, C. SENEMAUD, M. L. THEYE, J. BULLOT, M. GALIN, M. GAUTHIER, B. BOURDON and M. TOUL-EMONDE, *Solid State Commun.* **45** (1983) 649.

70. P. TRONC, M. BENSOUSSAN, A. BRENAC and C. SE-BENNE, *Phys. Rev.* **B8** (1973) 5947.

71. N. M. AMER and W. B. JACKSON, in "Hydrogenated Amorphous Silicon", edited by J. I. Pankove (Academic Press, New York, 1984). pp. 83–112.

72. M. L. THÉYE, M. F. KOTKATA, K. M. KANDIL, A. GHEORGHIN, C. SENEMAND, J. DIXMIER and F. PRA-DAL, *J. Non-Cryst. Solids* **137** (1991) 963.